ADVANCED FUNCTIONAL MATERIALS
www.afm-journal.de

Vapor-Phase Deposition of Monofunctional Alkoxysilanes for Sub-Nanometer-Level Biointerfacing on Silicon Oxide Surfaces

By *Brian Dorvel, Bobby Reddy Jr., Ian Block, Patrick Mathias, Susan E. Clare, Brian Cunningham, Donald E. Bergstrom,* and *Rashid Bashir**

Improving the performance and lowering the analyte detection limits of optical and electronic biosensors is essential for advancing wide ranging applications in diagnostics and drug discovery. Most sensing methods require direct linkage of a recognition element and a sensor, which is commonly accomplished through an organic monolayer interface. Alkoxyorganosilanes are typically used to prepare sensor surfaces on dielectric oxides. However, many silanes lead to roughened or thick interfaces that degrade device sensitivity. Here, controlled vapor phase deposition of monoalkoxysilanes is found to lead to monolayers resistant to elevated temperatures and extreme pH conditions. The formation of high density, subnanometer monolayers is demonstrated by ellipsometry, XPS, and AFM. The uniform attachment of these monofunctional silanes to such biosensing platforms as microarrays, field effect devices, and the formation of surface enhanced Raman spectroscopy substrates is demonstrated. The advantages of using this silane deposition protocol for the above technologies are also discussed.

1. Introduction

A typical biosensor contains three components; a receptor element, which recognizes or captures the biological or chemical analyte, the transducer, which converts the stimulus to an output signal, and an output system, which translates the output signal to an interpretable format. In the construction of biosensors, a variety of chemistries have been used to link receptor elements to surfaces; however, this step remains a limiting factor in device sensitivity, reliability, and reproducibility.[1,2] The output signal relies on transduction by optical,[3–7] electrochemical,[8–10] or piezoelectric techniques,[11] or other methods, and hence sensitivity increases with proximity of the analyte to the surface. Consequently, the linkage distance from the surface to the receptor elements must be reduced in order to maximize the contributions to the signal from the bound analyte. Self-assembled monolayers (SAMs) are commonly employed for interfacing biological receptors to a transducer. Many optical and electrochemical methods contain oxides, which are effective substrates for conjugation of alkoxy- and halo-substituted organosilanes, as part of the transducer. The mechanism of their reaction with oxide surfaces has been well studied,[12] and their aqueous and thermal stabilities have been established.[1,2,13,14]

Self-assembled monolayers are commonly deposited through either liquid- or vapor-based methods. There has been some success in the formation of trialkoxysilane monolayers in solution phase[15] and by using dip pen lithography,[16,17] but there exists much room for improvement. There is a need to make the deposition processes simpler and more reliable, to reduce the generation of contaminated effluents and polymerized products, and to lower the production costs.[18] Processes which utilize vapor-phase deposition can eliminate some of the problems that are seen in liquid-based deposition and also make themselves amenable to be used in batch and microelectronics-compatible processes.[19,20] In these vapor-phase processes, the precursor chemistry is easily controlled and efficient mass transport ensures coating of high-aspect-ratio structures (such as those found in micro-electro-mechanical devices). Moreover, it has been shown that the

[*] Prof. R. Bashir, B. Dorvel, B. Reddy Jr., I. Block, P. Mathias, Prof. B. Cunningham
Micro and Nanotechnology Laboratory
208 North Wright Street Urbana, Illinois 61801 (USA)
E-mail: rbashir@illinois.edu

Prof. R. Bashir, B. Reddy Jr., I. Block, P. Mathias, Prof. B. Cunningham
Department of Electrical and Computer Engineering
University of Illinois Urbana-Champaign
Urbana, IL 61801 (USA)

Prof. R. Bashir, Prof. B. Cunningham
Department of Bioengineering
University of Illinois at Urbana-Champaign
Urbana, IL 61801 (USA)

B. Dorvel
Department of Biophysics and Computational Biology
University of Illinois Urbana-Champaign
Urbana, IL 61801 (USA)

Prof. S. E. Clare
Indiana University School of Medicine
Indianapolis, IN 46202 (USA)

Prof. D. E. Bergstrom
Department of Medicinal Chemistry and Molecular Pharmacology
Birck Nanotechnology Center
Purdue University
West Lafayette, IN 47097 (USA)

DOI: 10.1002/adfm.200901688

© 2010 WILEY-VCH Verlag GmbH & Co. KGaA, Weinheim
WILEY InterScience® DISCOVER SOMETHING GREAT

performance of SAM coatings that are grown in vapor phase is comparable or superior to SAMs that are grown in liquid phase,[21] and the vapor phase methods can be applied at the wafer scale level.[22] Indeed, vapor-phase deposition of trialkoxysilane SAMs with a variety of terminal functional groups has been achieved on oxide surfaces previously.[23–28] However, these trifunctional silanes are also known to polymerize in either aqueous- or vapor-phase deposition methods over a wide range of temperatures and environmental conditions.[29–33] Consequently, high-quality monolayer formation may require very stringent and specialized processing conditions, making them more challenging to integrate with very-large-scale integration (VLSI) or wafer scale microelectronic devices and processes.

Organosilanes with trifunctional reactive groups, such as octadecyltrichlorosilane and aminopropyltriethoxysilane, have been frequently conjugated to devices by vapor and liquid methods,[34–37] with the latter silane of particular importance because the amino group allows simple conjugation to reactive functional groups, including active esters, aldehydes, and ketones and isocyanates.[38] However, the possible difficulties with trialkoxysilanes mentioned earlier may compromise device performance by causing nonuniformities on the active areas of the sensor or by increasing the length of the interfacial region. Monofunctional silanes possess the ability to alleviate these issues, since only one functional group is available to react with the surface and since these films have been shown to successfully be deposited on oxide surfaces.[39,40] Other added advantages include a higher vapor pressure than equivalent trifunctional silanes and the fact that these monofunctional silanes do not displace amine catalysts unless covalent linkage occurs. These advantages allow for extended high temperature deposition and curing times, variables known to influence the quality and robustness of the films, as well as facilitating vapor-phase deposition, which is the preferred passivation method in the semiconductor industry. However, to date only limited characterization has been performed on monofunctional silanes and little is known about their performance in solution or applicability to biosensing platforms.

In the present study, we evaluate vapor-phase deposition of two monoethoxysilanes, one amino-terminated and another glycidoxy-terminated, and demonstrate their applicability to biosensor fabrication. The kinetics of monolayer formation was measured with ellipsometry and found to follow a diffusion-limited Langmuir model. X-Ray photoelectron spectroscopy (XPS) confirmed the elemental compositions of completed monolayers. Atomic force microscopy (AFM) images of the complete monolayers suggest roughness values close to that of silicon, and the topography indicated high density coverage. A critical issue surrounding these monolayers is their aqueous stability under stressed conditions, particularly at elevated temperatures, and extreme pH values. To assess the stability, the aminoalkyl-derived surface was first allowed to react with an amine-reactive fluorophore. The fluorescent intensities were then compared for monolayers subjected to temperatures of 25 °C and 60 °C, and aqueous solution pH values ranging from 1 to 13 for time periods up to 6 hours. No measureable changes in fluorescence intensity and fluorescence uniformity were observed.

Subsequently, we applied this deposition method to optical and electrochemical biosensing platforms, including microarrays, field-effect devices, and surface enhanced Raman spectroscopy (SERS)-active substrates. We show the high deposition uniformity and decreased background noise when applied to microarrays. We also demonstrate that the conjugation technique can be applied to field-effect devices for possible applications in potentiometric sensing. Finally, we demonstrate high coverage densities of Au nanoparticles for the formation of SERS-active substrates for Raman detection capabilities. Overall, the ease of this functionalization method and its high stability show promise for increasing the performance and longevity of biosensors. As a result, this silanization can be widely applied across many biosensing platforms.

2. Results

Since monofunctional silane reaction kinetics has seldom been studied,[39] we deposited silanes for various time intervals in the vapor phase using the procedure described in the Experimental Section and then removed any physisorbed material by sonication. This allows for a more accurate determination of the extent of silane reaction as compared to real-time measurements such as quartz crystal microbalance (QCM) or surface plasmon resonance (SPR), since fluidic rinses or gaseous purges may not desorb excess reagents leading to an overestimation of silane attachment.[41] The ellipsometric thickness of the silane layer versus the deposition time is displayed for 3-aminopropyldimethylethoxysilane (APDMS) and (3-glycidoxy)propyldimethylethoxysilane (GPDMS) in Figure 1. Assuming that the film is uniform, the adsorbed mass can be correlated to the thickness if the molar refractivity and refractive index of the film are known.[42] The molar refractivity (A) of molecular species may be calculated by summation of the individual atomic bond refractivities which comprise the molecule. The molar refractivities for APDMS ($A = 35.4$) and GPDMS ($A = 49.1$) were calculated using the individual bond refractivities reported by Vogel et al.[43] and the adsorbed mass was calculated for each point. The right axis in Figure 1 shows the theoretical adsorbed mass for each silane. For both silanes, the thickness results indicate the deposition follows Langmuir kinetics. The first hour is dominated by rapid kinetics and as the adsorption sites become occupied, the deposition slows and finally saturates between 6–12 hours. Using trifunctional silanes with epoxy and amino functionalities, we performed the same deposition procedures, which readily gave multilayers with thicknesses in agreement with recent literature values (see Supporting Information).[30] Contact-angle measurements were also taken at the same deposition times (see Supporting Information), and the values saturate at 49.5° and 58.0° for APDMS and GPDMS, respectively.

Although the early stages of monolayer adsorption are known to be described well by Langmuir kinetics,[44,45] extended depositions have been known to follow second-order or diffusion-limited forms of the Langmuir model with several growth process regimes.[46] In order to gain insight into the deposition mechanism, the data was fit using three Langmuir models: a first order process, a second-order process, and a diffusion limited process. By analyzing the residuals of the fit, the kinetics appear to follow a diffusion limited process which is described well by Rahn and Hallock.[47] Using this model, the maximum thickness and diffusion-limited rate constant (k_{1D}) were calculated

© 2010 WILEY-VCH Verlag GmbH & Co. KGaA, Weinheim

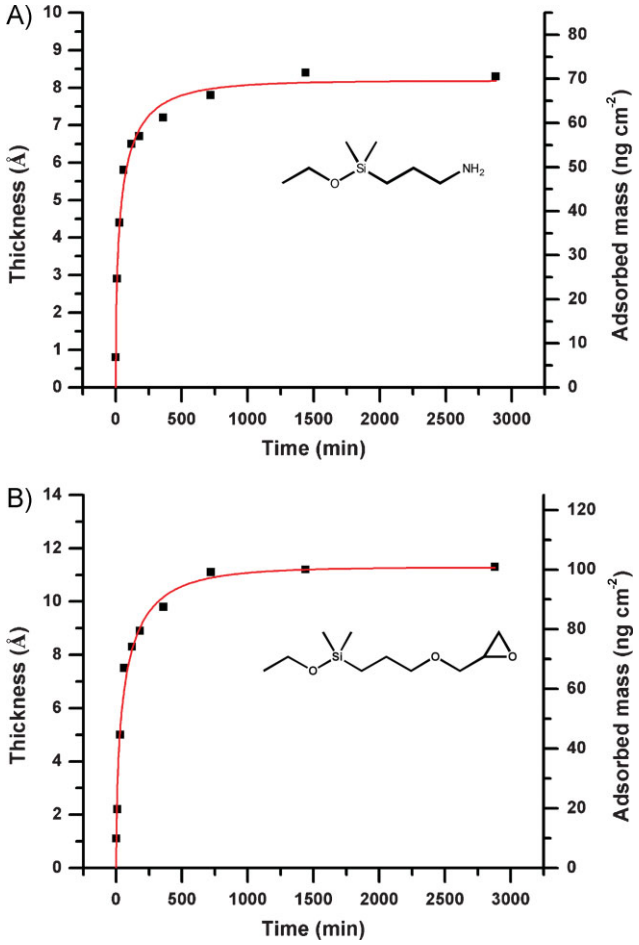

Figure 1. The thickness of APDMS (A) and GPDMS (B) versus deposition time as measured by ellipsometry. The points are fit to a diffusion-limited Langmuir equation (red line) for each molecule.

and are displayed in Table 1 for the aminosilane and epoxysilane. A purely diffusion limited process should be described by Equation 1:

$$\Gamma(t) \approx \Gamma_f \left(1 - \exp^{(\tau/\tau_D)^{1/2}}\right) \quad (1)$$

where τ_D is the diffusion-limited time constant and Γ_f is the final thickness. To evaluate the validity of the model, the power exponent of 1/2 in the equation was turned into a stretched exponential creating the exponent variable α. By allowing α to be a parameter in the fit, the optimal values of α were determined for APDMS and GPDMS. The values are displayed in Table 1, and both are close to 1/2, indicating a true diffusion limited process for the vapor deposition. The theoretical adsorbed masses saturate at 101.6 ng cm^{-2} and 69.8 ng cm^{-2} for the GPDMS and the APDMS, respectively. Taking the molecular weights of the compounds, this corresponds to 5.8 molecules nm^{-2} for the epoxysilane and 6.1 molecules nm^{-2} for the aminosilane. The high densities described for both silanes are not unreasonable, given the density of silanols achievable on crystalline silicon surfaces.[48,49] By cleaning the substrates properly and depositing the silanes at 100 °C, we are able to inhibit dehydroxylation at the surface, and maximize surface silanol density.

The vapor deposition of these silanes in vacuum and at temperature above their boiling points allows for simultaneous deposition and curing, with curing known to play an important role in stabilizing the attachment of the silane to the surface.[1,50] The ellipsometry results indicate saturated values for both monolayers by 12 hours deposition time. To confirm the compositions of the monolayers and correlate the ellipsometry thicknesses, XPS was taken for each silane after 12 hours deposition time. Figure 2 shows the C1s and N1s high-resolution spectra for a native oxide control, APDMS, and GPDMS. Within each spectrum, the curves were fitted to extract the localized bonding of each carbon or nitrogen atom. The native oxide shows very little carbon or nitrogen contamination, confirming that the signal results from the C1s and N1s of the attached silanes. The C1s spectra for each of the silanes contain binding energies for aliphatic (284.5–285.5 eV), slightly polar (286–287 eV), and highly polar (288–290 eV) carbons. The N1s spectra are split into NH_2 (399 eV) and NH_3^+ (401 eV) domains, which suggests that the amino groups of APDMS exist in both neutral and protonated form under the conditions of XPS analysis.

The ratios of each of the elements and the ratios of the carbon types are displayed in Table 1. The C1s:N1s ratio provides information about the elemental composition of the silanes. For APDMS, the ratio is close to the stoichiometric value of 5:1, while GPDMS, which does not contain nitrogen, has a very high C1s:N1s ratio. Similarly, the ratio of aliphatic carbons (C_a) to slightly polar carbons (C_p) can give us insight into the chemical composition of the sample. Slightly polar carbons may be regarded as O−C−O, C−O, or C−N bonded, while aliphatic carbons are assigned as C−C or C−H bonded. The C_a:C_p values for GPDMS and APDMS are very close to the stoichiometric values of 1:1 and 4:1, respectively. Most importantly, if the silane layer was damaged or oxidized during the long deposition time, the highly polar C1s peaks, indicating C=O or C=N, would be quite large. There is no evidence of this in the C1s spectra of either silane, indicating intact functional groups after the 12 hour deposition/curing period.

The N1s spectrum for APDMS shows greater than 97% NH_2 terminations. This is an important result, since it indicates that the

Table 1. Table of values for a 12 hour deposition period of APDMS and GPDMS. The various parameters gathered from ellipsometry, XPS, AFM, and contact angle are tabulated above.

	Ellipsometric Thickness (Å)	XPS Thickness (Å)	k_{1D} (min$^{-1/2}$)	α	$\frac{C1s}{N1s}$	$\frac{C-C}{C-O/C-N}$	R_{RMS} (Å)	Contact Angle (θ)
APDMS	8.2±0.4	8.6±0.8	0.15	0.52	5.08	4.11	1.6	49.5
GPMS	11.1±0.5	11.7±1.1	0.11	0.48	192.12	1.12	2.1	58.0

© 2010 WILEY-VCH Verlag GmbH & Co. KGaA, Weinheim

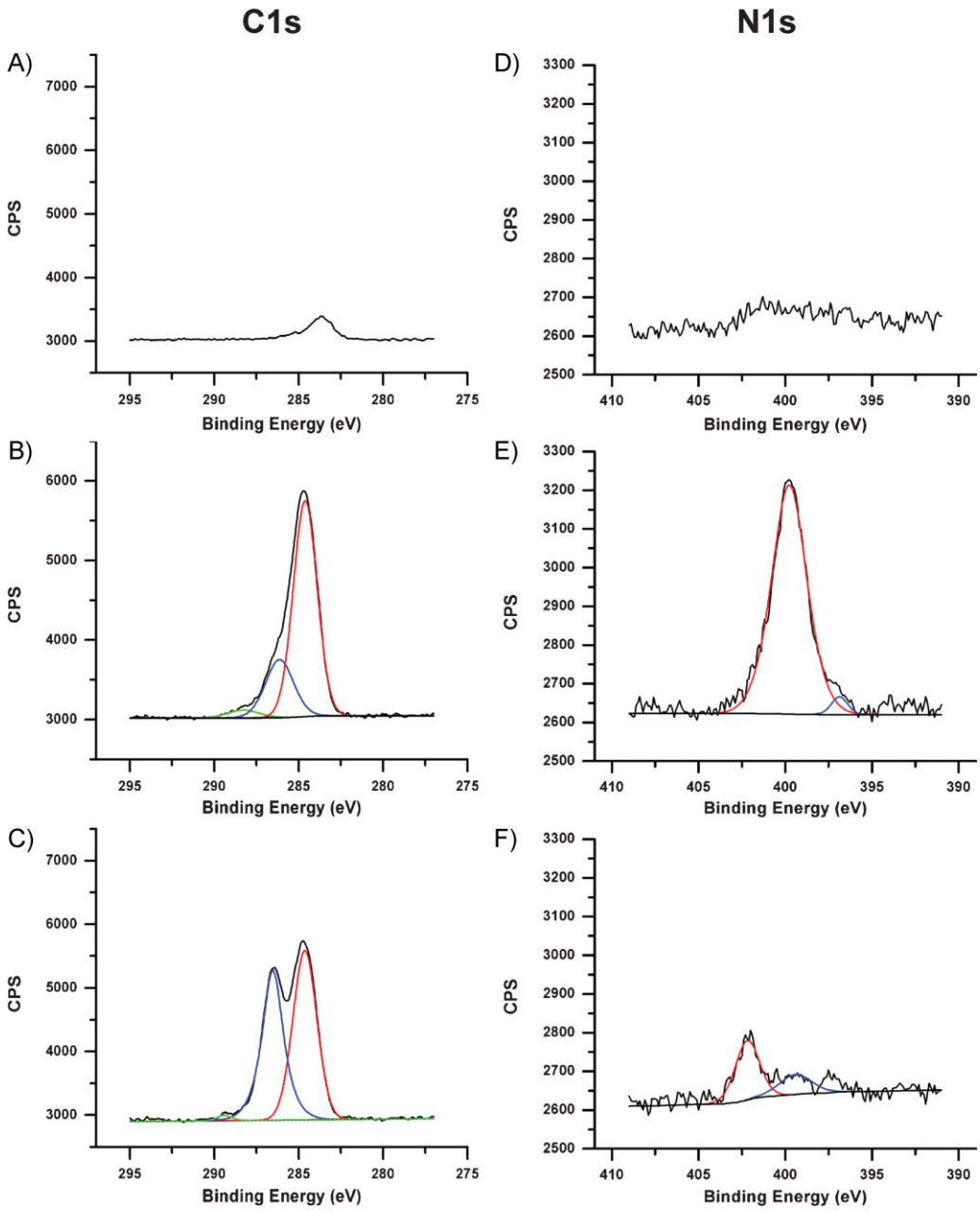

Figure 2. XPS high-resolution spectra of C1s (A–C) and N1s (D–F) peaks after 12 hours deposition time. A blank substrate (A, D) shows little carbon or nitrogen contamination. The APDMS spectra for C1s (B) are curve fitted to show the peak assignments C—C (red), C—N (blue), and C=N (green) regions. The APDMS N1s spectra (E) show the peak assignments NH_2 (red) and silicon bound nitrogen (blue). The GPDMS spectra for C1s (C) shows the peak assignments C—C (red), C—O (blue), and C=O (green), while the N1s spectra (F) shows traces of adsorbed nitrogen gas (red) and protonated nitrogen (blue).

silanes on the surface are covalently attached instead of absorbed in the inverted state. In an inverted state, the silane would form an $NH_3^+Si{-}O^-$ ion pair, which commonly occurs in trifunctional silanes such as APTES.[51,52] Moreover, the data also indicates that triethylamine is not absorbed on the surface, which would block binding sites. The N1s spectra of GPDMS show peaks close to the noise of the control spectrum, as would be expected. The thickness (t) of the monolayers was calculated by Equation 2 from the intensity of the Si2p electrons from the substrates (I) and the attenuation length of a hydrocarbon monolayer (λ):

$$t = -\lambda \sin\theta \ln\left(\frac{I}{I_o}\right) \tag{2}$$

where I_0 is the Si2p electron intensity from a blank sample and $\sin\theta$ reflects the take-off angle, which is 90°, making $\sin\theta$ equal to 1. The attenuation length for the electrons in the hydrocarbon

© 2010 WILEY-VCH Verlag GmbH & Co. KGaA, Weinheim

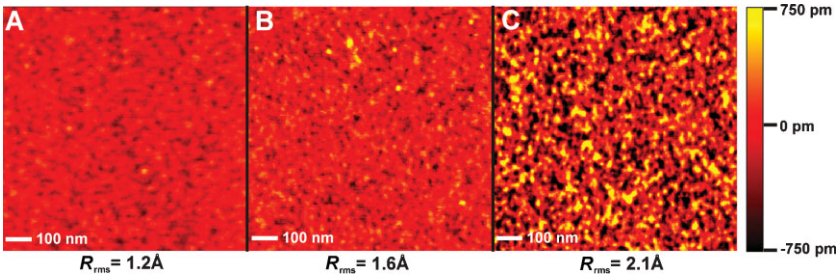

Figure 3. AFM tapping mode images of a native oxide substrate (A), an APDMS-coated substrate after 12 hours deposition (B), and a GPDMS-coated substrate after 12 hours deposition (C). The scale bar for all images is located on the right. The root mean square roughness (R_{rms}) values for the substrates are displayed below each image.

layer is dependent upon the kinetic energy of the electron being ejected, which for an Si2p electron is 1 388 eV. The attenuation length as a function of kinetic energy $\lambda(KE)$ was estimated for a hydrocarbon layer based upon the equation by Laibinis et al.,[53] that is, $\lambda(KE) = 9 + 0.022KE$. Using this equation, the attenuation length was estimated at 39.5 Å for the monolayer. The thicknesses were then calculated using Equation 2, and are displayed in Table 1. For both silanes, the XPS appears to overestimate, but within error, the thickness of the silanes, in comparison to ellipsometry. However, both techniques complement each other and support the formation of a true, high density monolayer.

The morphologies of the formed monolayers were visualized using AFM in tapping mode after 12 hours deposition. The results of the AFM are displayed in Figure 3 for the control oxide, APDMS, and GPDMS. The morphologies look quite similar to the control image, lacking island domains which would be indicative of incomplete monolayers or solution-phase depositions. Below each image is the RMS roughness (R_{rms}) for that image, and the values may also be found in Table 1. The control oxide exhibits an R_{rms} of 1.2 Å, which is well known to be the case for native oxides on silicon, while APDMS and GPDMS exhibit R_{rms} values of 1.6 Å and 2.1 Å, respectively. The fact the R_{rms} values are so close to the control and less than the heights of the molecules affirm the formation of homogeneous layers. Although the GPDMS R_{rms} is larger than APDMS, this is to be expected since the overall length of the molecule is longer and has a greater tendency to aggregate. AFM images were also taken for the same deposition times for their trifunctional analogues, showing large multilayer domains and R_{rms} values larger than the lengths of the molecules (see Supporting Information).

To demonstrate applicability of this vapor-based method to the semiconductor industry, both APDMS and GPDMS were deposited on 6-inch Si wafers with <100> silicon orientation. The deposition time for each silane was also 12 hours and took place in a 0.75 foot^3 vacuum oven with 1 mL of silane for each deposition. The ellipsometric thickness and static contact angle was taken over 25 spots on each wafer, and the wafer maps for APDMS and GPDMS can be found in the Supporting Information as Figure S3. The values indicate a thickness of 8.3 ± 0.4 Å and a contact angle of $50.3 \pm 2.1°$ for APDMS, while GPDMS had a thickness of 11.0 ± 0.8 Å and a contact angle of $58.9 \pm 2.6°$. These values over entire 6-inch Si wafers match, within the standard deviation, the values determined with 4×7 mm test chips. Moreover, the standard deviations are less than 10% of the mean value, indicating highly uniform depositions over large areas are achievable using this process. To gain insight into the resistance of the monolayers to hydrolysis, APDMS was subjected to various conditions over a period of 6 hours, and then allowed to react with a ROX-NHS ester. The fluorescence was then measured and is displayed over a period of 6 hours in Figure 4. Figure 4A shows the fluorescent intensity after incubation in 0.1 M HCl and 0.1 M NaOH. There is little decrease in fluorescent intensity over 6 hours for both solutions, and is within the error of each measurement. A similar experiment was performed but with the silanes incubated in pH 7.4 phosphate-buffered saline (PBS) at 60 °C and 90 °C and is shown in Figure 4B. Again, the fluorescent intensity decay is within the errors of the measurement for both solutions. Overall, Figure 4 demonstrates

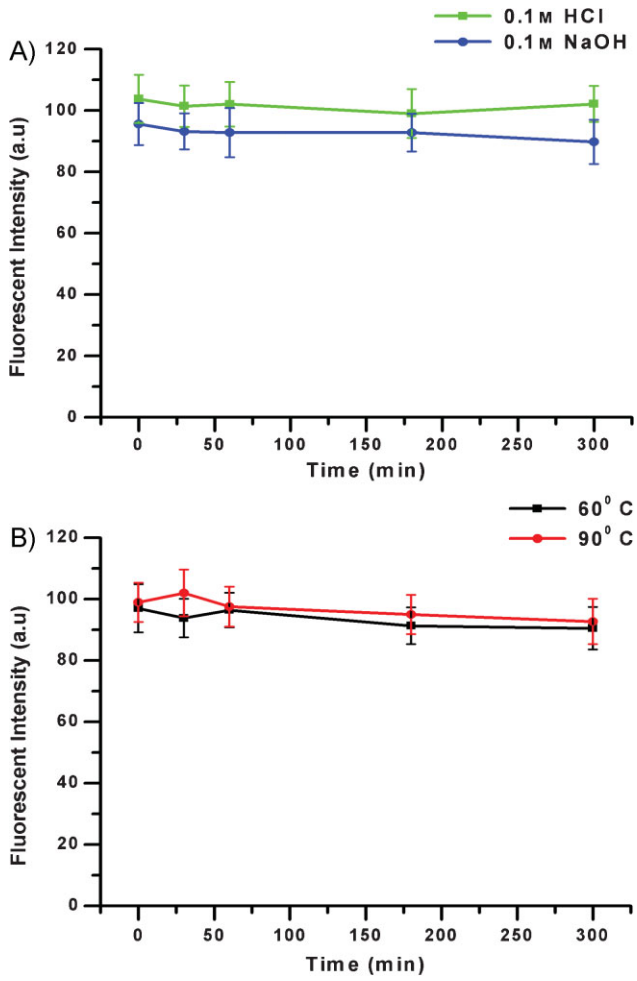

Figure 4. Substrates coated with APDMS over a 12 hour deposition period were subjected to 0.1 M HCl and 0.1 M NaOH (A) for up to 6 hours, allowed to react with rhodamine NCS for 1 hour, and then the fluorescent intensity measured. Similarly, substrates were immersed in pH 7.4 PBS buffer at 60 °C and 90 °C (B) for up to 6 hours, allowed to react with rhodamine NCS for 1 hour, and then the fluorescent intensity measured. The integration time for each measurement was 5 seconds.

© 2010 WILEY-VCH Verlag GmbH & Co. KGaA, Weinheim

ADVANCED FUNCTIONAL MATERIALS
www.afm-journal.de

Materials Views
www.MaterialsViews.com

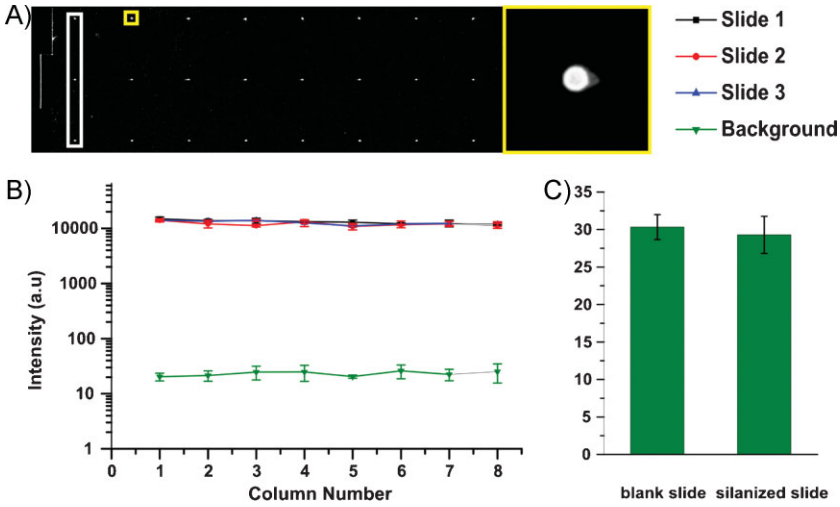

Figure 5. Low-autofluorescence microscope slides were coated with GPDMS over a 12 hour period and then spotted with Streptavidin-Cy5 in a volume of 350 pL. A representative slide spotted in a 3 × 8 array is shown in (A) showing a single column (white rectangle) and a magnified image of an individual spot (yellow square). The fluorescence intensity of each column and its surrounding background are shown for three slides in (B). The intensity is plotted on a logarithmic scale. The background of a bare slide versus a GPDMS slide is shown in (C), indicating no difference in background within experimental error.

the resistance of the monolayers to harsher conditions than one would encounter in the ambient. This behavior of monofunctional silanes has been observed before, and is believed to be due to increased reactivity with surface hydroxyl groups.[54]

Next, the monolayers were applied to biosensing devices to demonstrate their versatility and application. Figure 5A shows a GPDMS-coated microscope slide spotted with streptavidin-Cy5 (SA-Cy5) in a 3 × 8 array format. The columns are boxed in white, with a zoomed-in area of an individual spot in yellow. Each pixel of the scan was 10-μm square. Three slides were spotted in the same manner and scanned to obtain the fluorescence intensity of the spots and the background. Figure 5B shows the intensity of the background and of the SA-Cy5 spots for each slide versus the column number. The intensity distribution of fluorescence and uniformity of background noise from the columns across all three slides is very uniform. The background noise of a silane-derivatized slide and an underivatized slide were also measured, and are displayed in Figure 5C. The silane adds no background fluorescence, within error, to the measurement. Given the high gain of the photomultiplier tube at which these measurements were taken, it is likely that background noise due to substrate autofluorescence and the detection electronics will dominate over background contributions from the silane layer for any fluorescence assay. The low autofluorescence of these layers is an important advantage in ultimately maximizing the signal-to-noise ratio of fluorescence assays performed using this chemistry, and apparently leads to better background intensity than other slide formats.[55] The coefficient of variation across the slides is 8%, which includes effects from the variability of the spotting procedure as well as the surface chemistry.

The application of ion-selective field-effect transistors (ISFETs) and silicon nanowires to biosensing has become pronounced in recent years.[56–58] Silicon oxide is the most common dielectric due to its ease of growth and integration. However, silicon oxide performance is known to degrade extensively over time, due to factors such as dissolution and ion diffusion.[59–62] Organic monolayers have proven to provide resistance to this phenomena,[38] but the effect of polymerization degrades the device sensitivity by adding to the dielectric thickness and trapping charges within the polymerized matrix. Moreover, functional group density may be affected due to groups being buried in the matrix. These variables may affect the ability of the silane chemistry to conjugate recognition agents, such as primary antibodies or DNA, close enough to the surface to regulate the devices surface potential. Here, we demonstrate the applicability and versatility of monoalkoxysilylation chemistry to biosensors. We have constructed silicon field effect devices based upon silicon-on-insulator (SOI) technology in our lab[63,64] with 30-nm silicon thickness, 2-μm device width, and 20-μm device length. A bright-field top-view micrograph of a device is displayed in Figure 6 (top left). We allowed the devices to react with the monofunctional silylating reagents according to the aforementioned protocol, and then with fluorophores of varying functionalities, including an amine, an NHS ester, and an isothiocyanate. Each device was then fluorescently imaged for 5 seconds (Fig. 6). The presence of the fluorophores is demonstrated by the uniformly strongly intensity across the device. Since device response can depend on the distribution of recognition molecules on the surface,[65] this is an important step to optimizing silicon nanowire sensitivity and repeatability.

Another important technique widely used today for biomolecule detection is SERS. Interactions of analytes with enhanced optical fields are known to increase Raman scattering by 10^5–10^6. In some cases, scattering enhancements of 10^{12}–10^{14} have been encountered, which may be sensitive enough for single-molecule detections. Former SERS substrates were made out of electrochemically roughened metal surfaces, but in recent years noble metal nanoparticles have become a method of choice. Nanoparticle substrates offer the advantage of being renewable and having a high density of particles on the surface, which can lead to areas of intense field enhancement known as ''hot spots''.[66] In Figure 7, we demonstrate the formation of high-density Au nanoparticle surfaces via electrostatic adsorption with an APDMS monolayer. AFM images were taken before (Fig. 7A) and after (Fig. 7B) a 1 hour deposition of 5-nm Au particles in deionized (DI) water. Figure 7A shows a smooth monolayer over a 25-um^2 area. After deposition (Fig. 7B), the surface shows a high density of Au nanoparticles on the surface over the same area scale. A 1-μm^2 image of the same area shows particles in tight clusters, with occasional gaps. A line scan across one of these small gap areas shows a height difference of 5.7 nm, indicating a homogeneous monolayer of nanoparticles.

WILEY InterScience DISCOVER SOMETHING GREAT
© 2010 WILEY-VCH Verlag GmbH & Co. KGaA, Weinheim

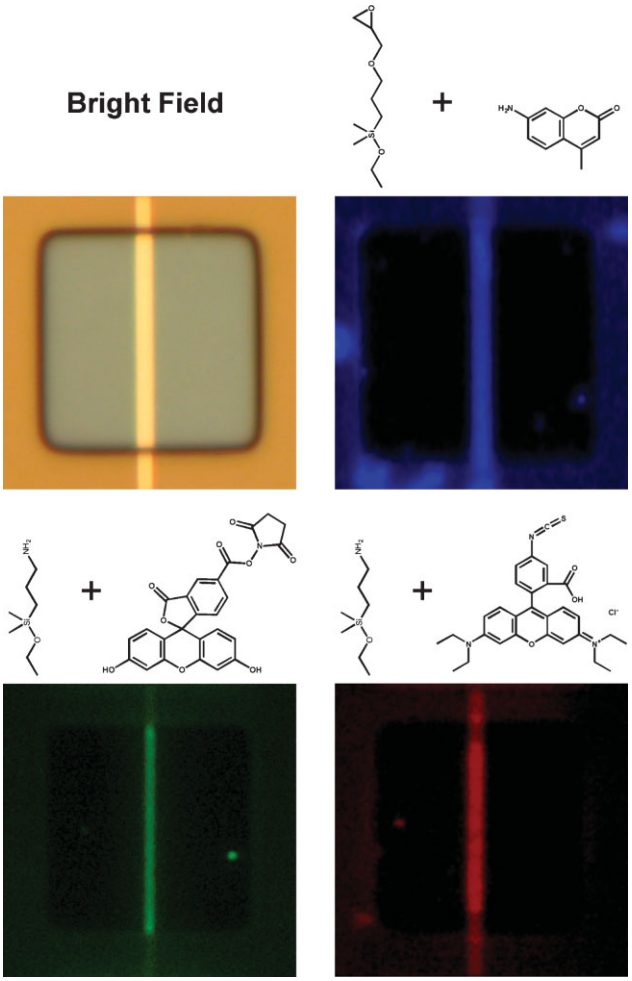

Figure 6. Silicon field-effect devices were silanized and then reacted with fluorophores of varying chemistries. The bright field image shows a silanized device (metallic yellow) in the center of the release window, which shows the buried oxide (blue–violet). The devices were then allowed to react with various fluorophores, which are indicated atop each fluorescence image, along with the silane utilized for conjugation. The fluorophores reacted include an amino-coumarin (top, right), carboxyfluorescein-NHS ester (bottom, left), and rhodamine B-isothiocyanate (bottom, right).

3. Conclusions

We have developed a versatile, vapor-based method for the deposition of monofunctional silanes. By characterizing the system using ellipsometry, XPS, and AFM we were able to optimize the procedure to ensure a uniform, high density, true monolayer. The technique was shown to be successful not only on small substrates, such as ISFET's, but also on entire 6-inch Si wafers, leaving the possibility for incorporation into VLSI semiconductor processes. Subjecting the monolayers to conditions of elevated temperatures and extreme pH showed no decay of the monolayers through fluorescent attachment. We demonstrate the applicability of this subnanometer monolayer technology to various sensing platforms. The very high uniformity of the monolayers makes them ideal for applications in sensing, whether optically or electronically based. The low background noise and coefficient of variation make it attractive for microarrays and fluorescence applications. Moreover, the chemistry indicates recognition analytes would bind in high density to field-effect sensors, enhancing the sensitivity of the devices. Finally, the high coverage of electrostatically adsorbed nanoparticles on the silane surface would make an ideal SERS substrate for detection of analytes and minimize background scattering. Overall, the deposition of monofunctional silanes is very versatile and robust, and is applicable to multiple biosensing platforms to help optimize their performance.

4. Experimental

Materials: APDMS and GPDMS were purchased from Gelest, Inc. and used without further purification. Triethylamine, toluene, and methanol were obtained from Sigma and dried with 3A molecular sieves. The fluorescent dyes 7-amino-4-methylcoumarin, rhodamine B isothiocyanate, and 4-carboxyfluorescein NHS-ester were purchased from Sigma–Aldrich and used without further purification. pH 7.4 PBS was purchased from Gibco and degassed at 30 Torr in a desiccator for 10 minutes prior to use. All glassware prior to use was soaked in a NaOH:EtOH base bath for at least one hour and rinsed in DI water. The glassware was then dried at 150 °C in a convection oven. Four-inch Si(100) wafers from SiliconQuest Intl. were diced into 4 × 7 mm chips for AFM, XPS, and ellipsometry experiments. A 4-inch Si(100) wafer was thermally oxidized at 1 050 °C for 24 hours to an SiO_2 thickness of ~1 μm, which was confirmed by ellipsometry, and then diced into 4 × 7 mm chips for fluorescence-stability measurements. Low-autofluorescence Nexterion B microscope slides purchased from Schott were used for deposition uniformity experiments. Streptavidin-Cyanine-5 (SA-Cy5) for microarray spotting was purchased from Invitrogen. Silicon field-effect devices were fabricated in our lab using SOI wafers and a VLSI-compatible process [63,64]. Colloidal Au nanoparticles (Au-NPs) of 5-nm mean diameter were purchased from Sigma and used as received.

Silane Deposition: Before silane depositions, each substrate was degreased in acetone and methanol, then immersed in H_2SO_4:H_2O_2 (7:3) for 30 minutes. The substrates were then rinsed in DI water, dried under a stream of N_2, and then subjected to a 300 W O_2 plasma at a pressure of 500 mTorr for 10 minutes. The deposition of silanes on 4 × 7 mm chips was performed in 20 cm^3 glass vials at a temperature of 100 °C and at a pressure of 30 Torr. Silanes were mixed with TEA to a 1% v/v solution, kept at 100 °C and 30 Torr, and transferred into the vials by a glass

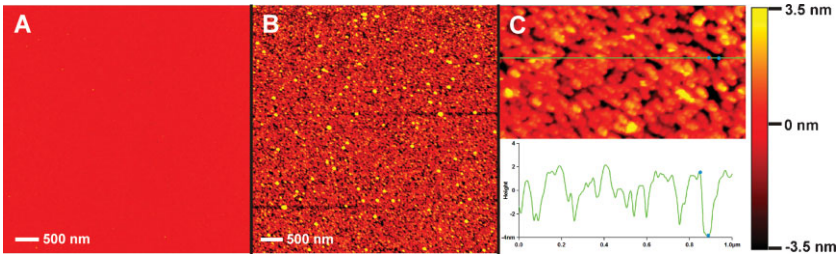

Figure 7. A 5-μm tapping mode AFM image of an APDMS-coated substrate is shown in (A). An APDMS substrate was then coated with citrate-capped 5-nm Au nanoparticles over a period of 1 h and a 5-μm image taken in (B), showing very high coverage. A 1-μm image of the same area is shown in (C) with a line section taken (green). The section analysis shows a height difference of 5.7 nm, indicating a true monolayer of particles on the surface.

© 2010 WILEY-VCH Verlag GmbH & Co. KGaA, Weinheim

syringe using an 18-gauge stainless steel hypodermic needle through a viton septum. The reactions were quenched by purging the vials with N_2 at least 3 times. Chips were removed from the vials and then sonicated in vials containing toluene and methanol for 2 minutes each, respectively. The chips were then dried under a stream of N_2 for 5 minutes and stored in a vacuum desiccator until use.

Microscope slides and 6-inch Si wafers were prepared in a 0.75 foot^3 vacuum oven equipped with an N_2 and a vacuum port, preheated to 100 °C. The slides were mounted horizontally in a glass rack which contained a rectangular bottom well for the silane solution. A volume of 1-mL silane solution was deposited in the bottom well and the rack was evacuated to a pressure of 30 Torr. The slides were subjected to the silane vapor for 12 hours. After 12 hours, the reaction was quenched by 3 purges with N_2 and then vacuum. The slides were then removed from the glass rack and sonicated in baths of toluene and methanol for 2 minutes, respectively. The slides were then rinsed with deionized water and dried under a stream of N_2 for 5 minutes.

The 6-inch Si wafers were silanized using the same vacuum oven setup and same conditions, except the N_2 inlet port was modified with a t-junction for carrying the silane vapor from outside the oven. The silane was put in a fused silica vial with a vacuum port to a total volume of 1 mL, connected to the t-junction via polytetrafluoroethylene (PTFE) tubing, and heated on a hot plate. A copper heating tape was put around the PTFE tubing to ensure isothermal conditions for the vapor leading into the chamber. The vacuum oven, PTFE tubing, and the silane were all preheated to 100 °C, and the 6-inch wafer inserted into the vacuum oven. The oven was purged with N_2 and then vacuumed out 3 times. The t-junction was then opened to allow the silane to flow into the vacuum oven for 12 hours. After the deposition, the t-valve was closed to the silane and N_2 was cycled in to quench the reaction 3 times. The wafer was then removed from the oven and sonicated in toluene and methanol for 2 minutes each. The wafers were then carefully dried with a stream of N_2 to avoid spotting.

Silane Characterization: The ellipsometry measurements were taken on a Rudolph FE-III ellipsometer at an angle of 70° and a wavelength of 6328 Å. The refractive indices utilized were 1.46 for the native oxide and 1.43 for the silanes. The chips were measured before and after silanization at 5 different spots. The native oxides for each dye ranged from 10–14 Å in thickness, as determined by ellipsometry and XPS. Contact-angle measurements were taken on a KSV CAM200 system in static mode using the sessile drop technique. A 10-uL drop of ultrapure water (18.2 MΩ cm) was allowed to stabilize for 10 minutes before the measurement was taken. Error for each measurement is approximately ± 0.5 degrees. TOF-SIMS XPS analysis was done on a KRATOS AXIS ULTRA at a take-off angle of 90°. Monochromatic $Al_{k\alpha}$ X-rays were used as the source. The control sample was carefully cleaned to remove carbonaceous material according to Seah and Spencer [67]. Silanized samples were subjected to a similar treatment, but without the use of O_2/plasma to keep the monolayer intact. Survey spectra were taken at a pass energy of 120 eV and high-resolution spectra at a pass energy of 40 eV. Each dye was mounted using a conductive copper tape and the C1s, N1s, and Si2p spectra recorded at a dwell time of 200 ms and 10 passes. All spectra were processed using CASA XPS software. The spectra were fitted with a modified Gaussian–Lorenztian algorithm using a Shirley background.

Atomic force microscopy (AFM) images were taken on an Asylum Research MPF-3D AFM with a silicon tip at 300 kHz in AC Mode. The amplitude and phase images were both recorded and image sizes ranged from 1×1 μm to 5×5 μm. Microarray spotting was done using a non-contact piezoelectric spotter (Perkin Elmer Piezoarray) with a pattern containing 350-pL spots of 10 μg mL^{-1} SA-Cy5 in PBS at pH 7.4 with 0.05% trehalose to prevent spot drying. This SA-Cy5 concentration and volume equates to 70 attomol per spot. The spots were incubated at 4 °C for 12 h, rinsed in 0.1% Tween in PBS for 5 min with agitation, then briefly with dH_20. The spots were imaged with a fluorescence laser scanner (Tecan LS Reloaded) at a gain of 190 and a 10 μm pixel size. Processing of the collected images was performed using ArrayPro software to calculate trimmed-mean (10%) intensities of a 14-pixel-diameter region inside each spot. Background intensities were calculated as a trimmed-mean (10%) of the local corners around each spot. Images of silicon field-effect devices were taken on a Nikon TE20 fluorescent microscope with a Pixera 16 bit CCD camera. The integration time for each fluorescent image was 5 seconds.

Acknowledgements

We acknowledge the use of Micro and Nanotechnology Lab for device fabrication, and UIC NCS Staff for assistance with PECVD deposition. We are grateful to Intel Corporation for their helpful insight. This work was funded by NIH (R21-EB006308), NSF (ECS-0554990), a seed grant from the Indiana Elks administered through the Purdue University Cancer Center, and NIH (R01CA120003). Supporting Information is available online from Wiley InterScience or from the author.

Received: July 8, 2009
Published online: November 17, 2009

[1] M. A. Murphy, C. E. Nordgren, R. F. Fischetti, J. K. Blasie, L. J. Peticolas, J. C. Bean, *J. Phys. Chem.* **1995**, *99*, 14039.
[2] G. M. Whitesides, P. E. Laibinis, *Langmuir* **1990**, *6*, 87.
[3] J. Homola, *Chem. Rev.* **2008**, *108*, 462.
[4] X. D. Fan, I. M. White, S. I. Shopoua, H. Y. Zhu, J. D. Suter, Y. Z. Sun, *Anal. Chim. Acta* **2008**, *620*, 8.
[5] J. N. Anker, W. P. Hall, O. Lyandres, N. C. Shah, J. Zhao, R. P. Van Duyne, *Nat. Mater.* **2008**, *7*, 442.
[6] A. K. Bhunia, P. Banada, P. Banerjee, A. Valadez, E. D. Hirleman, *J. Rapid Methods Autom. Microbiol.* **2007**, *15*, 121.
[7] M. E. Bosch, A. J. R. Sanchez, F. S. Rojas, C. B. Ojeda, *Comb. Chem. High Throughput Screening* **2007**, *10*, 413.
[8] D. Grieshaber, R. MacKenzie, J. Voros, E. Reimhult, *Sensors* **2008**, *8*, 1400.
[9] M. Vestergaard, K. Kerman, E. Tamiya, *Sensors* **2007**, *7*, 3442.
[10] S. Rauf, J. J. Gooding, K. Akhtar, M. A. Ghauri, M. Rahman, M. A. Anwar, A. M. Khalid, *J. Pharm. Biomed. Anal.* **2005**, *37*, 205.
[11] K. Lange, B. E. Rapp, M. Rapp, *Anal. Bioanal. Chem.* **2008**, *391*, 1509.
[12] J. Sagiv, *J. Am. Chem. Soc.* **1980**, *102*, 92.
[13] V. Depalma, N. Tillman, *Langmuir* **1989**, *5*, 868.
[14] S. R. Wasserman, Y. T. Tao, G. M. Whitesides, *Langmuir* **1989**, *5*, 1074.
[15] J. A. Howarter, J. P. Youngblood, *Langmuir* **2006**, *22*, 11142.
[16] H. Jung, R. Kulkarni, C. P. Collier, *J. Am. Chem. Soc.* **2003**, *125*, 12096.
[17] S. Naoto, N. Jun, E. Yoshitaka, H. Atsushi, M. Yoshitake, I. Shigeru, S. Yoshio, *Adv. Funct. Mater.* **2008**, *18*, 3049.
[18] R. Maboudian, W. R. Ashurst, C. Carraro, *Tribol. Lett.* **2002**, *12*, 95.
[19] W. R. Ashurst, C. Carraro, R. Maboudian, *IEEE Trans. Device Mater. Reliab.* **2003**, *3*, 173.
[20] M. P. de Boer, T. M. Mayer, *MRS Bull.* **2001**, *26*, 302.
[21] T. M. Mayer, M. P. de Boer, N. D. Shinn, P. J. Clews, T. A. Michalske, *J. Vac. Sci. Technol. B* **2000**, *18*, 2433.
[22] W. R. Ashurst, C. Carraro, R. Maboudian, W. Frey, *Sens. Actuators, A* **2003**, *104*, 213.
[23] N. Saito, S. H. Lee, I. Takahiro, J. Hieda, H. Sugimura, O. Takai, *J. Phys. Chem. B* **2005**, *109*, 11602.
[24] A. Hozumi, Y. Yokogawa, T. Kameyama, H. Sugimura, K. Hayashi, H. Shirayama, O. Takai, *J. Vac. Sci. Technol. A* **2001**, *19*, 1812.
[25] A. Hozumi, K. Ushiyama, H. Sugimura, O. Takai, *Langmuir* **1999**, *15*, 7600.
[26] L. Hong, H. Sugimura, T. Furukawa, O. Takai, *Langmuir* **2003**, *19*, 1966.
[27] Y. Miura, H. Sato, T. Ikeda, H. Sugimura, O. Takai, K. Kobayashi, *Biomacromolecules* **2004**, *5*, 1708.
[28] A. Hozumi, M. Inagaki, N. Shirahata, *Surf. Sci.* **2006**, *600*, 4044.
[29] J. Kim, P. Seidler, C. Fill, L. S. Wan, *Surf. Sci.* **2008**, *602*, 3323.
[30] J. Y. Kim, P. Seidler, L. S. Wan, C. Fill, *J. Colloid Interface Sci.* **2009**, *329*, 114.
[31] Q. L. Gu, X. H. Cheng, *Curr. Appl. Phys.* **2008**, *8*, 583.
[32] K. C. Vrancken, P. Vandervoort, K. Possemiers, E. F. Vansant, *J. Colloid Interface Sci.* **1995**, *174*, 86.

© 2010 WILEY-VCH Verlag GmbH & Co. KGaA, Weinheim

[33] K. M. R. Kallury, P. M. Macdonald, M. Thompson, *Langmuir* **1994**, *10*, 492.
[34] L. S. Jang, H. J. Liu, *Biomed. Microdevices* **2009**, *11*, 331.
[35] V. K. S. Hsiao, J. R. Waldeisen, Y. B. Zheng, P. F. Lloyd, T. J. Bunning, T. J. Huang, *J. Mater. Chem.* **2007**, *17*, 4896.
[36] B. Baur, J. Howgate, H. G. von Ribbeck, Y. Gawlina, V. Bandalo, G. Steinhoff, M. Stutzmann, M. Eickhoff, *Appl. Phys. Lett.* **2006**, *89*, 183901.
[37] A. B. Kharitonov, M. Zayats, A. Lichtenstein, E. Katz, I. Willner, *Sens. Actuators, B* **2000**, *70*, 222.
[38] J. A. Voorthuyzen, K. Keskin, P. Bergveld, *Surf. Sci.* **1987**, *187*, 201.
[39] L. D. White, C. P. Tripp, *J. Colloid Interface Sci.* **2000**, *232*, 400.
[40] S. M. Kanan, W. T. Y. Tze, C. P. Tripp, *Langmuir* **2002**, *18*, 6623.
[41] J. J. R. Stalgren, J. Eriksson, K. Boschkova, *J. Colloid Interface Sci.* **2002**, *253*, 190.
[42] P. A. Cuypers, J. W. Corsel, M. P. Janssen, J. M. M. Kop, W. T. Hermens, H. C. Hemker, *J. Biol. Chem.* **1983**, *258*, 2426.
[43] A. I. Vogel, W. T. Cresswell, J. Leicester, *J. Phys. Chem.* **1954**, *58*, 174.
[44] O. Dannenberger, K. Weiss, C. Woll, M. Buck, *Phys. Chem. Chem. Phys.* **2000**, *2*, 1509.
[45] O. Dannenberger, K. Weiss, H. J. Himmel, B. Jager, M. Buck, C. Woll, *Thin Solid Films* **1997**, *307*, 183.
[46] K. A. Peterlinz, R. Georgiadis, *Langmuir* **1996**, *12*, 4731.
[47] J. R. Rahn, R. B. Hallock, *Langmuir* **1995**, *11*, 650.
[48] L. Boksanyi, O. Liardon, E. S. Kovats, *Adv. Colloid Interface Sci.* **1976**, *6*, 95.
[49] B. Humbert, *J. Non-Cryst. Solids* **1995**, *191*, 29.
[50] M. CalistriYeh, E. J. Kramer, R. Sharma, W. Zhao, M. H. Rafailovich, J. Sokolov, J. D. Brock, *Langmuir* **1996**, *12*, 2747.
[51] A. A. Golub, A. I. Zubenko, B. V. Zhmud, *J. Colloid Interface Sci.* **1996**, *179*, 482.
[52] B. V. Zhmud, A. B. Pechenyi, *J. Colloid Interface Sci.* **1995**, *173*, 71.
[53] P. E. Laibinis, C. D. Bain, G. M. Whitesides, *J. Phys. Chem.* **1991**, *95*, 7017.
[54] C. P. Tripp, M. L. Hair, *Langmuir* **1995**, *11*, 149.
[55] S. L. Seurynck-Servoss, A. M. White, C. L. Baird, K. D. Rodland, R. C. Zangar, *Anal. Biochem.* **2007**, *371*, 105.
[56] E. Stern, J. F. Klemic, D. A. Routenberg, P. N. Wyrembak, D. B. Turner-Evans, A. D. Hamilton, D. A. LaVan, T. M. Fahmy, M. A. Reed, *Nature* **2007**, *445*, 519.
[57] Y. Cui, Q. Q. Wei, H. K. Park, C. M. Lieber, *Science* **2001**, *293*, 1289.
[58] Y. Cui, Z. H. Zhong, D. L. Wang, W. U. Wang, C. M. Lieber, *Nano Lett.* **2003**, *3*, 149.
[59] G. Zhang, *Electrochemistry of Silicon and its Oxide, Kluwer*, Academic, New York **2001**.
[60] H. Abe, M. Esashi, T. Matsuo, *IEEE Trans. Electron Devices* **1979**, *26*, 1939.
[61] T. Matsuo, M. Esashi, H. Abe, *IEEE Trans. Electron Devices* **1979**, *26*, 1856.
[62] T. Matsuo, M. Esashi, *Sens. Actuators* **1981**, *1*, 77.
[63] O. H. Elibol, B. Reddy, R. Bashir, *Appl. Phys. Lett.* **2008**, *92*, 193904.
[64] O. H. Elibol, D. Morisette, D. Akin, J. P. Denton, R. Bashir, *Appl. Phys. Lett.* **2003**, *83*, 4613.
[65] P. R. Nair, M. A. Alam, *IEEE Trans. Electron Devices* **2007**, *54*, 3400.
[66] W. Y. Li, P. H. C. Camargo, X. M. Lu, Y. N. Xia, *Nano Lett.* **2009**, *9*, 485.
[67] M. P. Seah, S. J. Spencer, *J. Vac. Sci. Technol. A* **2003**, *21*, 345.

© 2010 WILEY-VCH Verlag GmbH & Co. KGaA, Weinheim